Monthly Notices of the ROYAL ASTRONOMICAL SOCIETY

MNRAS **525,** 4143–4148 (2023)
Advance Access publication 2023 August 7

https://doi.org/10.1093/mnras/stad2244

Statistical analysis of the onset temperature of solar flares in 2010–2011

Douglas Félix da Silva,[1,2]★ Li Hui,[1,3] Paulo J. A. Simões ,[2,4]★ Adriana Valio ,[2] Joaquim E. R. Costa,[5] Hugh S. Hudson ,[4,6] Lyndsay Fletcher ,[4,7] Laura A. Hayes[8] and Iain G. Hannah[4]

[1]*State Key Laboratory of Space Weather, National Space Science Center, Chinese Academy of Sciences, Beijing 100190, China*
[2]*Center for Radio Astronomy and Astrophysics Mackenzie, Engineering School, Mackenzie Presbyterian University, São Paulo 01301000, Brazil*
[3]*University of Chinese Academy of Sciences, Beijing 101408, China*
[4]*SUPA School of Physics and Astronomy, University of Glasgow, Glasgow G128QQ, UK*
[5]*National Institute for Space Research (INPE), São Jose Dos Campos 12227010, Brazil*
[6]*Space Sciences Laboratory, UC Berkeley 94720 CA, USA*
[7]*Rosseland Centre for Solar Physics, University of Oslo, PO Box 1029 Blindern, NO-0315 Oslo, Norway*
[8]*European Space Agency (ESA), European Space Research and Technology Centre (ESTEC), Keplerlaan 1, 2201 AZ Noordwijk, The Netherlands*

Accepted 2023 July 19. Received 2023 June 29; in original form 2022 December 1

ABSTRACT

Understanding the physical processes that trigger solar flares is paramount to help with forecasting space weather and mitigating the effects on our technological infrastructure. A previously unknown phenomenon was recently identified in solar flares: the plasma temperature, derived from soft X-ray (SXR) data, at the onset of four flares, was revealed to be in the range 10–15 MK, without evidence of gradual heating. To investigate how common the hot-onset phenomenon may be, we extend this investigation to solar flares of B1.2–X6.9 classes recorded by the X-ray Sensor (XRS) onboard the *GOES*-14 and *GOES*-15 satellites between 2010 and 2011. For this statistical study, we employed the same methodology as in recent work, where the pre-flare SXR flux of each flare is obtained manually, and the temperature and emission measure values are obtained by the flux ratio of the two *GOES*/XRS channels using the standard software. From 3224 events listed in the *GOES* flare catalogue for 2010–2011, we have selected and analysed 745 events for which the flare heliographic location was provided in the list, to investigate centre-to-limb effects of the hot-onset phenomenon. Our results show that 559 out of 745 flares (75 per cent) exhibit an onset temperature above 8.6 MK (the first quartile), with respective $\log_{10}$ of the emission measure values between 46.0–47.25 cm^{-3}, indicating that small amounts of plasma are quickly heated to high temperatures. These results suggest that the hot-onset phenomenon is very common in solar flares.

Key words: Sun: corona – Sun: flares – Sun: X-rays.

1 INTRODUCTION

Solar flares and coronal mass ejections (CME) are the most energetic transient events observed in the solar atmosphere. Solar flares are rapid and intense brightness variations of solar emission detected in all electromagnetic spectrum, whereas CMEs consist of large amounts of magnetized plasma ejected into interplanetary space.

Flares occur within active regions in the solar atmosphere, and the released energy is believed to be of magnetic origin. Due to magnetic reconnection, which facilitates the release of stored magnetic energy, flares accelerate particles, heat the local plasma, and produce radiation at all wavelengths (Benz 2008; Fletcher et al. 2011). Predicting when a major solar event will occur is crucial to mitigate the possible effects of space weather on our planet. One way to do this is to better understand the causes of solar activity phenomena. Hence, studying the plasma conditions before the impulsive phase of a solar flare may clarify the physical processes that occur leading up to the main flare energy release.

Hudson et al. (2021) analysed a set of four flares observed in soft X-rays (SXR) by the X-ray Sensor (XRS) onboard the *Geostationary Operational Environmental Satellite* (*GOES*) and discovered that, at the onset of these events, the initial plasma temperature T inferred from the SXR data was already high, around 10–15 MK. The associated emission measure EM values were low (EM < 10^{47} cm^{-3}), suggesting that a small volume of plasma was quickly heated to such high temperatures. The temperature and emission measure were inferred from the ratio of the flux between the two SXR channels, 1–8 Å and 0.5–4 Å, following White, Thomas & Schwartz (2005), and confirmed by X-ray spectroscopic analysis of *Reuven Ramaty High Energy Solar Spectroscopic Imager* (Lin et al. 2002) observations of the same events. Using ultraviolet images from the *Atmospheric Imaging Assembly* (Lemen et al. 2012) onboard the *Solar Dynamics Observatory* (Pesnell, Thompson & Chamberlin 2012), the authors identified the location and size of the flare sources during this onset interval, and concluded that the 10–15 MK plasma originated from very compact, low-lying, and short-lived features.

Such hot, compact volumes of plasma have been previously observed both in SXR (Hudson et al. 1994; Mrozek & Tomczak 2004) and extreme ultraviolet (EUV; Fletcher et al. 2013; Graham et al. 2013; Simões, Graham & Fletcher 2015), but during the impulsive

★ E-mail: douglas93f@gmail.com (DFdS); paulo@craam.mackenzie.br (PJAS)

phase of flares. During the impulsive phase, these compact sources are well-associated spatially with the flare ribbons, and display an impulsive behaviour, before the coronal SXR and EUV emissions dominate.

The immediately high temperature, between 10 and 15 MK, at the beginning of the event is a characteristic of the hot onset observed in the SXR data. A gradual heating from the minimum detection of GOES, of 4 MK, to the flare temperature to identify any period of. Hudson et al. (2021) show that these compact events occur in the low-solar corona. We do not know if this is common for all events.

In this work, we aim to verify how common the hot-onset phenomenon occurs in solar flares. For this, we analyse the events recorded by the *GOES* satellite between 2010 and 2011.

The data selection criteria and methodology are described in Section 2. We discuss the results in Section 3. Finally, the main conclusions are presented in Section 4.

2 TEMPERATURE AND EMISSION MEASURE AT THE ONSET OF SOLAR FLARES

2.1 Data selection

We analysed solar flares that occurred between 2010 and 2011 and were detected in SXR by the *GOES*-14 and *GOES*-15 satellites. The standard routines to obtain and process *GOES*/XRS data, part of thes solar software package (ssw, Freeland & Handy 1998), a software library for solar analysis written in IDL, was used to obtain and reduce the data. To carry out this work, we used data from the Solar Data Analysis Center at NASA Goddard Space Flight Center.

In May 2022, a critical note, regarding the temperature and emission measurements calculations from *GOES* XRS data, reports that the treatments of *GOES*-13 through 15 have been corrected due to an erroneous assumption about the calibration performed previously in solarsoft. Thus any temperatures and emission measures calculated within SSW for *GOES*-13 through 17 before May 2022 are now considered incorrect by up to 30 per cent. Our analysis was done before these changes, so we chose not to consider the changes to maintain exactly the same calibration as in (Hudson et al. 2021) for comparison. We warn that future work should take this into account.

Using the SSW routine `get_gev.pro`, we obtained the *GOES* flare list between 2010 and 2011 (the beginning of Cycle 24), with 3224 solar flares, including B-class events. The data, also obtained via solarsoft tools, incorporate the recent *GOES* database recalibrations (Peck et al. 2021). The selection of the pre-flare time interval is usually performed by a researcher, a time-consuming method that hinders the statistical analysis of very large samples. In Section 2.2, we discuss our approach to a straightforward and standardized background subtraction. We do note that an automated method was presented by Ryan et al. (2012), the Temperature and Emission measure-Based Background Subtraction method (TEBBS). A comparison between our method and TEBBS is beyond the scope of the current paper and will be presented in the future.

In addition to characterizing the emission measure and temperature at the onset of the selected events, we also investigated whether centre-to-limb effects are present. Therefore, the heliographic location of each flare was also collected from the list. From the original 3224 events, 906 flares had a reported location. We further discarded 157 events, where the pre-flare flux of one of the channels (usually the high-energy one) was below the detection limit of the *GOES*/XRS. Our final sample contained 745 events for the analysis: 6 X-class flares, 69 M-class, 524 C-class, and 146 B-class events.

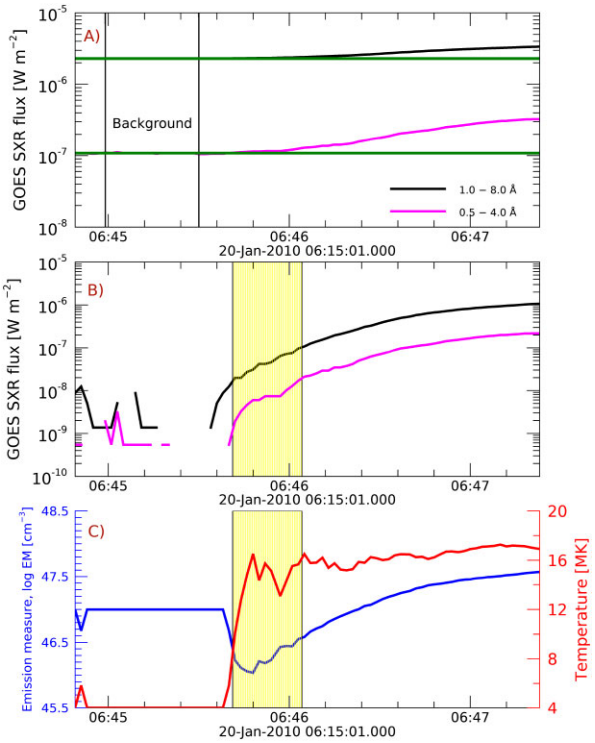

Figure 1. Initial phase of the SOL2010-02-20T06:45 event. **(A)** The *GOES* flux in the 1–8 Å band (magenta curve) and in 0.5–4Å (black curve) are shown. The vertical black lines limit the background time interval. The green horizontal lines depict the average flux estimated within the background time interval. **(B)** The background subtracted flux in the 1–8 Å band (magenta curve) and in 0.5–4Å (black curve). The yellow strip is the interval chosen for the 'onset' interval, which in this case has a 20 s duration. **(C)** The calculated temperature and emission measure of the SXR source. The red curve represents the temperature (right *y*-axis) evolution during the flare, whereas the emission measure is shown in blue (left *y*-axis).

2.2 Background selection, temperature and emission measure estimates

To obtain the temperature T and emission measure EM at the onset of the selected events, only the excess flux emission during each solar flare's beginning must be considered. We manually carried out the pre-flare flux levels (background) subtraction procedure for each of the 745 analysed events. This process consisted of two steps: (1) identify the start time of the solar flare and (2) select a time interval before the event's start. In the first step, we visually identified the beginning of each event; the parameters of the *GOES* list only helped us find the events in the observation light curve. To obtain the background value, we use the average flux of the chosen background time interval, for each channel respectively.

An example of the application of the methodology to obtain the T and EM of each flare is given in Fig. 1. Fig. 1a shows the initial phase of the SOL2010-02-20T06:45 event. The vertical lines mark the chosen pre-flare time interval with respect to the *GOES* flux for the channels 1–8 Å (black line) and 0.5–4 Å (magenta line); the green lines mark the average flux within the background window denoted in Fig. 1a. The flux excess of both SXR channels are shown in Fig. 1b, where we identify the flare onset: the instant where both SXR channels display values above the pre-flare flux (i.e. positive values). As discussed below, the onset interval, marked by the yellow region, was chosen to be 20 s.

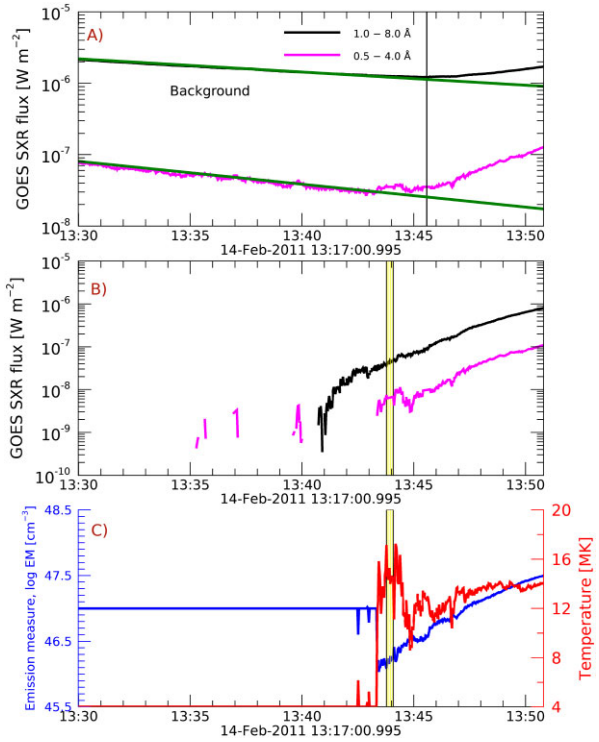

Figure 2. The initial phase of the SOL2011-02-14T13:44 event. The same as Fig. 1, but with the background flux modelled as an exponential function. This was necessary because this flare occurred during the decay phase of a previous event.

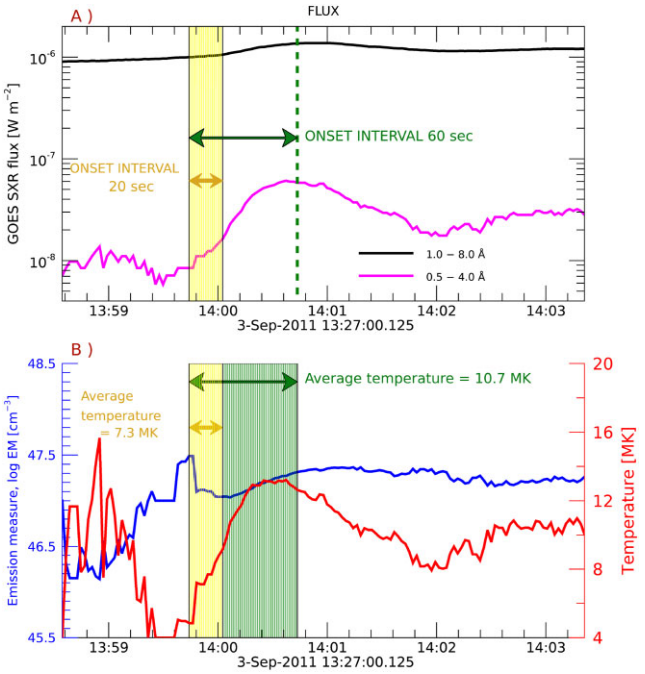

Figure 3. Comparison of onset time intervals of 20 and 60 s (indicated by the horizontal arrows), for the event SOL2011-09-03T13:27UT. (a) SXR flux for the 1–8 Å band (black curve) and in 0.5–4Å (magenta curve) both with background and (b) temperature T and emission measure EM derived from the SXR data. Note that the 60 s interval captures the instant of a maximum flux of the event and the peak temperature, indicating that this choice of onset interval is inadequate. The average temperature in the 60-s interval (10.7 MK) is higher than that of the 20-s interval (7.3 MK) because, for short events, the 60-s interval includes the start event to the peak.

Finally, Fig. 1c shows the time evolution of the plasma temperature T (red) and emission measure EM (blue) as obtained via the standard routines (White et al. 2005). The onset T and EM are calculated by taking the average of these quantities in the onset time interval. Note that the temperature is already above 10 MK within the first twenty seconds of the event; this characterizes a hot-onset event.

Some flares start during the gradual phase of a previous event. For these cases, the time variation of the pre-flare flux can be fitted by an exponential function (i.e. a straight line in log space), under the assumption that this model captures both the flux of the gradual phase of the previous event and the flux contribution from the rest of the Sun. Note that we only applied the exponential fit method to flares that occurred during the gradual phase of a previous event. Fig. 2a shows an example of such a case, SOL2011-02-14T13:17, where the flux in the background interval for each *GOES*/XRS channel is fitted with an exponential function (green line). Fig. 2b and 2c show the excess flux and the resulting T and EM, the same as Fig. 1. It was necessary to employ this procedure for 130 events (of out 745) in our sample.

We decided to adopt a fixed onset interval of 20 s. The choice for the onset time interval is somewhat arbitrary but a necessary one for a robust statistical analysis. With a 20 s interval, there is enough data for averaging the T and EM values, with the XRS cadence of 2 s. With longer onset intervals, the rising phase and/or even the event's maximum might be captured. As an example, we compare two onset intervals: 20 and 60 s, shown in Fig. 3. The two intervals refer to a time interval measured forward from the start of the flare, as defined previously. Note that the 60-s interval (indicated by the green arrow) spans the beginning of the event until past its maximum. The resulting onset temperatures are $T(20\,\mathrm{s}) = 7.3$ MK and $T(60\,\mathrm{s}) = 10.7$ MK,

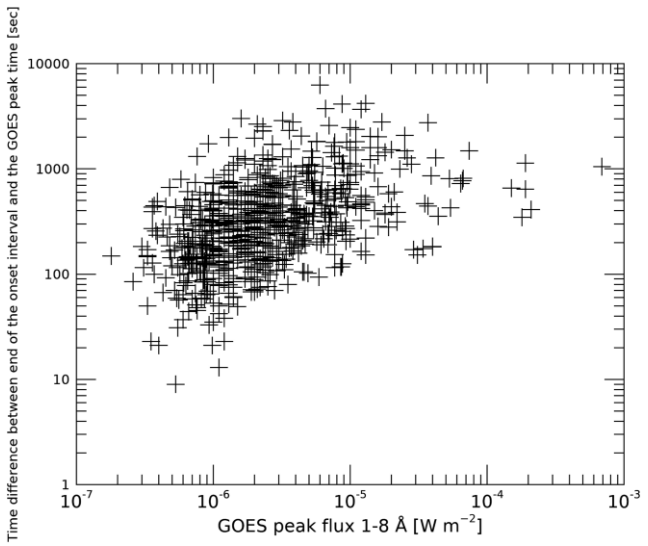

Figure 4. Time difference between the end of the selected onset time of 20 s and the *GOES* peak time for all analysed flares.

with the latter including the maximum temperature of the event. Thus, for short-duration events, a 60-s onset interval is too long. Therefore, a 20-s time interval is more appropriate for a statistical approach. We also checked whether the selected onset interval for each flare was sufficiently separated from the SXR peak time. In Fig. 4 we show the time difference between the end of the selected onset

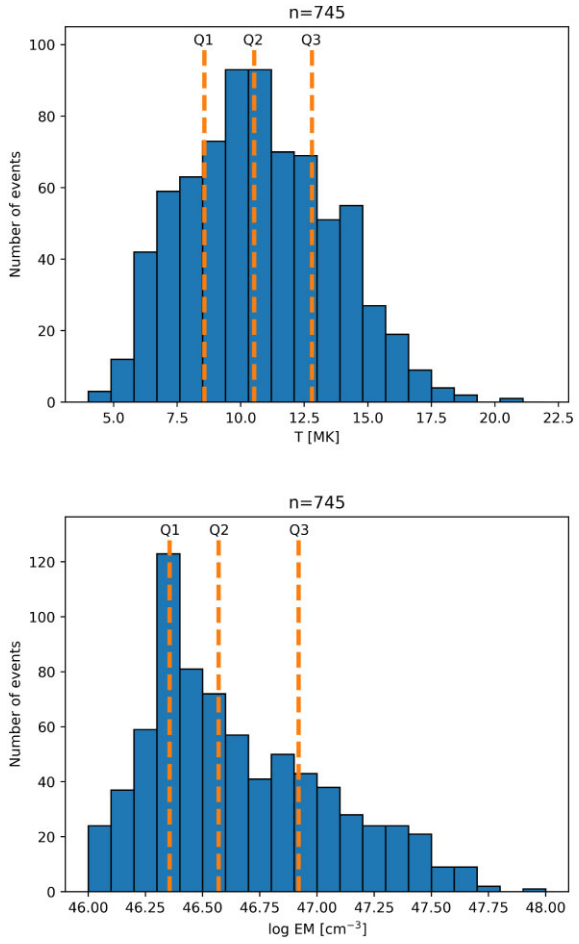

Figure 5. Distributions of the onset temperature (top panel) and emission measure (bottom panel) for the 745 flares in the period 2010–2011, considering a 20 s onset time interval. The vertical lines show the quartile values.

interval to the SXR peak time, for all analysed events. This time separation is well above tens of seconds for most events. All results showed hereafter were produced adopting an interval of 20 s for the onset.

3 RESULTS

3.1 Statistics of the onset *T* and EM

The temperature and the emission measure for all 745 events were calculated considering an onset interval of 20 s. Histograms of the onset temperature and the emission measure for all 745 events are shown in Fig. 5 in the top and bottom panels, respectively. The T distribution has a clear maximum of around 10 MK, and it is roughly symmetrical. The EM distribution also has a clear maximum, near $10^{46.3}$ cm^{-3}, but shows a longer tail towards higher values. We computed the quartiles of each distribution to quantify the interpretation of our results; these are indicated by the vertical lines in each panel of Fig. 5 and are presented in the Table 1.

We find that only ≈25% of our flare sample (186 events) have an onset temperature below 8.6 MK. The majority of the distribution presented onset temperatures that characterize a hot onset: 373 events with 8.6 MK $< T <$ 12.8 MK and 186 events with $T >$ 12.8 MK.

Table 1. Quartiles of the onset temperature and emission measure for 745 events.

Quartiles	Q1	Q2	Q3
T (MK)	8.6	10.5	12.8
Number of events	186	373	559
log EM (cm^{-3})	46.4	46.6	47.0
Number of events	187	374	599

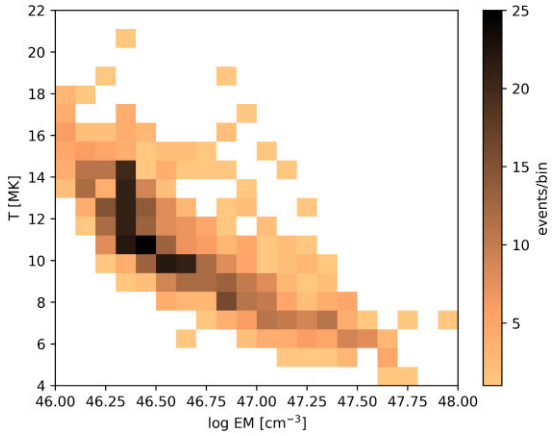

Figure 6. 2D histogram of the average temperature and emission measure estimated during the 20 s onset interval for the 745 analysed events.

These results show that 75 per cent of our sample (559 of 745 events) have an onset temperature above 8.6 MK. The sample presents a median temperature of 10.5 MK, within the initial 20 s from detecting SXR flux excess.

For the EM quartile analysis, 187 of the events have EM $<$ $10^{46.4}$ cm^{-3}, 412 events with 46.4 $<$ log EM $<$ 47.0, and 146 flares with log EM $>$ 47.0. These results indicate that only small amounts (EM $<$ 10^{48} cm^{-3}) of plasma are heated during the flare onset, as expected.

The correlation between temperature and emission measure at the onset of all the flares in our sample is shown in Fig. 6, which shows a 2D histogram of the distribution of EM and T. We see an anticorrelation between these quantities for the events, where the higher the emission measure, the lower the temperature. Most of the events are clustered between temperatures of 10–15 MK with EM $\sim 1.8 - 5.6 \times 10^{46}$ cm^{-3}.

3.2 Centre-to-limb effects on the onset *T* and EM

Hudson et al. (2021) show, in their Fig. 6, the onset temperature of flares occurring on the Active Region NOAA 11 748 during its appearance on the eastern limb. They conclude that the solar limb partially occults the flares before mid-day May 2013. Thus, the onset temperature (around or above 20 MK) is not the *true* temperature of the onset source (originating from compact, low-lying sources), but reflects the temperature of the emission from the coronal loops well into the evolution of the flare. As the Active Region (AR) rotates fully into view of the *GOES*/XRS sensors, the *true* onset temperatures are visible, yielding temperatures in the range of 10–15 MK.

To investigate this phenomenon, and any other centre-to-limb effects, we also analyse the onset temperature as a function of the solar longitude of each flare, as shown in Fig. 7. No correlation

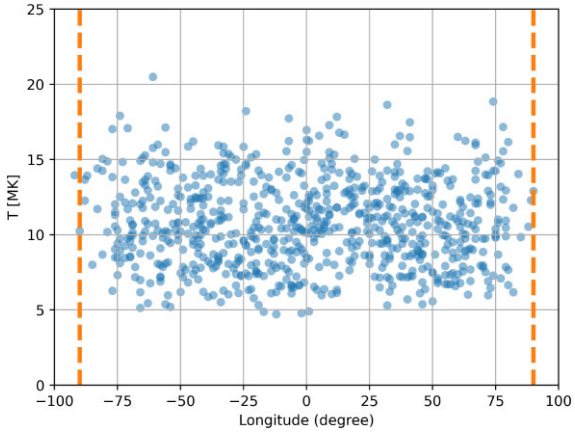

Figure 7. Average temperature during the onset of solar flares as a function of their longitude, as listed in the *GOES* catalogue. The orange vertical dashed lines mark the −90° and 90° maximum longitudes.

is seen between temperature and location of the flare, that is, no centre-to-limb variation is observed.

The four events analysed by Hudson et al. 2021 showed onset temperatures between 10 and 15 MK. The $T > 20$ MK onsets refer to the events of a single active region, as it rotated into view, in May 2013. We do not find similar temperatures in our sample of events; however, we also do not have a case of a limb-occulted flare, judging by the flare location data. As suggested by Hudson et al. 2021, the higher onset temperatures can be explained by detecting the SXR emission from the higher flares loops, already in an advanced phase of the flares. At the same time, the solar limb obscured the actual onset.

4 CONCLUDING REMARKS

Hudson et al. (2021) revealed the existence of high-temperature (10–15 MK) plasma, in small amounts (EM $< 10^{47}$ cm^{-3}), at the onset of four flares, ranging from classes B to M. These properties offer a new challenge for standard models and theoretical studies of the physics of solar flares.

To verify how common this newly revealed phenomenon is, we performed a statistical analysis of the temperature T and emission measure EM, obtained from the standard methodology from *GOES* XRS data, for flares in the period 2010–2011. *GOES*-14 and *GOES*-15 satellites observed over three thousand flares during this period. From this sample, we have analysed 745 events that had recorded, in addition to the *GOES* class, the start, peak, and end times, also the location and identification of the active region where the event occurred. This spatial information was important to locate the onset source on the solar disc.

Our results from a quartile analysis show that only 25 per cent of the flare sample had an onset temperature below 8.6 K, therefore, 75 per cent of our sample can be characterized as having a hot onset. The distribution of the onset temperatures for the 745 flares is unimodal, with a median of 10.5 MK. Also, there is a continuous distribution between the emission measure and temperature (see Fig. 6), where hotter events show a small contribution from the emission measure, and events with a lower temperature exhibit a larger emission measure value. The shape of this distribution results at least partially from the non-linear correlation between parameter uncertainties, which are roughly connected by $I \propto \mathrm{EM} \times e^{-\mathrm{const.}/T}$. The emission measures are generally tiny relative to their peak values, and the 20-s snapshots at the earliest times in the events have limited signal-to-noise ratios. The values in Fig. 6 suggest that, for most cases, small amounts of plasma are heated almost immediately to temperatures around 10 MK. Future studies with higher temporal and spatial resolutions may bring further information regarding the properties of the hot onset of flares. Only for 25 per cent of the flares in our sample is the initial temperature below 8.6 MK, where gradual heating can be observed during the initial phase of the events. Also, we find no centre-to-limb dependence of the onset temperature (Fig. 7).

Our study strongly indicates that the hot-onset phenomenon, revealed by Hudson et al. (2021), is a common feature of solar flares. Given the possible thermal nature of the hot onsets (Hudson et al. 2021), we anticipate that new clues might be obtained via observations in the infrared/THz range with the 30 THz cameras AR30T (López et al. 2022), BR30T (Giménez de Castro et al. 2018), and the new 15 THz *High Altitude THz Solar Telescope* (Giménez de Castro et al. 2020), soon to be operating at the Observatorio Astronómico Félix Aguilar, at the Argentinean Andes.

ACKNOWLEDGEMENTS

DFS acknowledges the support from the China-Brazil Joint Laboratory for Space Weather (CBJLSW). HL is supported by National Natural Science Foundation of China (NNSFC) grants (42022032, 41874203, and 42188101), International Partnership Programme of Chinese Academy of Sciences (CAS) (grant no. 183311KYSB20200017). PJAS acknowledges support from the Fundo de Pesquisa Mackenzie (MackPesquisa) and Conselho Nacional de Desenvolvimento Cientifico e Tecnologico (CNPq) (contract 307612/2019-8). This research was partially supported by Fundação de Amparo à Pesquisa do Estado de São Paulo (FAPESP) grant 2013/24155-3. LF acknowledges support from the UK's Science and Technology Facilities Council (grant no. ST/T000422/1). LF and IGH acknowledge support from the UK's Science and Technology Facilities Council (grant no. ST/T000422/1). LAH is supported by an ESA Research Fellowship.

DATA AVAILABILITY

All data used in this work reside in the public domain at https://umbra.nascom.nasa.gov/goes/fits/.

REFERENCES

Benz A. O., 2008, Living Rev. Sol. Phys., 5, 1
Fletcher L. et al., 2011, Space Sci. Rev., 159, 19
Fletcher L., Hannah I. G., Hudson H. S., Innes D. E., 2013, ApJ, 771, 104
Freeland S. L., Handy B. N., 1998, Sol. Phys., 182, 497
Giménez de Castro C. G., Raulin J. P., Valle Silva J. F., Simões P. J. A., Kudaka A. S., Valio A., 2018, Space Weather, 16, 1261
Giménez de Castro C. G. et al., 2020, Sol. Phys., 295, 56
Graham D. R., Hannah I. G., Fletcher L., Milligan R. O., 2013, ApJ, 767, 83
Hudson H. S., Simões P. J. A., Fletcher L., Hayes L. A., Hannah I. G., 2021, MNRAS, 501, 1273
Hudson H. S., Strong K. T., Dennis B. R., Zarro D., Inda M., Kosugi T., Sakao T., 1994, ApJ, 422, L25
Lemen J. R. et al., 2012, Sol. Phys., 275, 17
Lin R. P. et al., 2002, Sol. Phys., 210, 3

López F. M., Giménez de Castro C. G., Mandrini C. H., Simões P. J. A., Cristiani G. D., Gary D. E., Francile C., Démoulin P., 2022, A&A, 657, A51
Mrozek T., Tomczak M., 2004, A&A, 415, 377
Peck C., Machol J., Codrescu S., Zetterlund E., Rachmeler L., Viereck R., 2021, AGU Fall Meeting Abstracts, #SH25E
Pesnell W. D., Thompson B. J., Chamberlin P. C., 2012, Sol. Phys., 275, 3
Ryan D. F., Milligan R. O., Gallagher P. T., Dennis B. R., Tolbert A. K., Schwartz R. A., Young C. A., 2012, ApJS, 202, 11
Simões P. J. A., Graham D. R., Fletcher L., 2015, Sol. Phys., 290, 3573
White S. M., Thomas R. J., Schwartz R. A., 2005, Sol. Phys., 227, 231

This paper has been typeset from a TEX/LATEX file prepared by the author.